ISSN 1674-1056
http://cpb.iphy.ac.cn
http://iopscience.iop.org/cpb
中国物理 B
Chinese Physics
中国物理 Chinese Physics B

Thickness-modulated in-plane Bi_2O_2Se homojunctions for ultrafast high-performance photodetectors

Cheng-Yun Hong(洪成允)[1], Gang-Feng Huang(黄刚锋)[1], Wen-Wen Yao(要文文)[2], Jia-Jun Deng(邓加军)[2], Xiao-Long Liu(刘小龙)[1,3]

Citation: Chin. Phys. B . 2019, 28(12): 128502 . **doi:** 10.1088/1674-1056/ab4e87
Journal homepage: http://cpb.iphy.ac.cn; http://iopscience.iop.org/cpb

What follows is a list of articles you may be interested in

Metal halide perovskite photodetectors: Material featuresand device engineering

Ye Wang(王烨), Meng-Lei Gao(高孟磊), Jin-Liang Wu(吴金良), Xing-Wang Zhang(张兴旺)
Chin. Phys. B . 2019, 28(1): 018502 . **doi:** 10.1088/1674-1056/28/1/018502

Photon-counting chirped amplitude modulation lidar system using superconducting nanowire single-photon detector at 1550-nm wavelength

Hui Zhou(周慧), Yu-Hao He(何宇昊), Chao-Lin Lü(吕超林), Li-Xing You(尤立星), Zhao-Hui Li(李召辉), Guang Wu(吴光), Wei-Jun Zhang(张伟君), Lu Zhang(张露), Xiao-Yu Liu(刘晓宇), Xiao-Yan Yang(杨晓燕), Zhen Wang(王镇)
Chin. Phys. B . 2018, 27(1): 018501 . **doi:** 10.1088/1674-1056/27/1/018501

An improved design for AlGaN solar-blind avalanche photodiodes with enhanced avalanche ionization

Yin Tang(汤寅), Qing Cai(蔡青), Lian-Hong Yang(杨莲红), Ke-Xiu Dong(董可秀), Dun-Jun Chen(陈敦军), Hai Lu(陆海), Rong Zhang(张荣), You-Dou Zheng(郑有炓)
Chin. Phys. B . 2017, 26(3): 038503 . **doi:** 10.1088/1674-1056/26/3/038503

Analysis on high speed response of a uni-traveling-carrier double hetero-junction phototransistor

Jiang Zhi-Yun, Xie Hong-Yun, Zhang Liang-Hao, Zhang Wan-Rong, Hu Rui-Xin, Huo Wen-Juan
Chin. Phys. B . 2015, 24(4): 048504 . **doi:** 10.1088/1674-1056/24/4/048504

Zero-bias high-responsivity high-bandwidth top-illuminated germanium p–i–n photodetectors

Li Chong, Xue Chun-Lai, Liu Zhi, Cheng Bu-Wen, Li Chuan-Bo, Wang Qi-Ming
Chin. Phys. B . 2014, 23(3): 038506 . **doi:** 10.1088/1674-1056/23/3/038506

Thickness-modulated in-plane Bi_2O_2Se homojunctions for ultrafast high-performance photodetectors*

Cheng-Yun Hong(洪成允)[1], Gang-Feng Huang(黄刚锋)[1], Wen-Wen Yao(要文文)[2], Jia-Jun Deng(邓加军)[2], and Xiao-Long Liu(刘小龙)[1,3,†]

[1] *Renewable Energy School, North China Electric Power University, Beijing* 102206, *China*
[2] *Department of Mathematics and Physics, North China Electric Power University, Beijing* 102206, *China*
[3] *State Key Laboratory of Alternate Electrical Power System with Renewable Energy Sources and Beijing Key Laboratory of Energy Safety and Clean Utilization, North China Electric Power University, Beijing* 102206, *China*

(Received 22 August 2019; revised manuscript received 11 October 2019; published online 22 November 2019)

Bi_2O_2Se thin film could be one of the promising material candidates for the next-generation electronic and optoelectronic applications. However, the performance of Bi_2O_2Se thin film-based device is not fully explored in the photodetecting area. Considering the fact that the electrical properties such as carrier mobility, work function, and energy band structure of Bi_2O_2Se are thickness-dependent, the in-plane Bi_2O_2Se homojunctions consisting of layers with different thicknesses are successfully synthesized by the chemical vapor deposition (CVD) method across the terraces on the mica substrates, where terraces are created in the mica surface layer peeling off process. In this way, effective internal electrical fields are built up along the Bi_2O_2Se homojunctions, exhibiting diode-like rectification behavior with an on/off ratio of 10^2, what is more, thus obtained photodetectors possess highly sensitive and ultrafast features, with a maximum photoresponsivity of 2.5 A/W and a lifetime of 4.8 μs. Comparing with the Bi_2O_2Se uniform thin films, the photo-electric conversion efficiency is greatly improved for the in-plane homojunctions.

Keywords: Bi_2O_2Se, in-plane homojunction, thickness modulation, photodetectors

PACS: 85.60.Dw, 73.40.Lq, 71.20.Nr **DOI:** 10.1088/1674-1056/ab4e87

1. Introduction

Two-dimensional (2D) layered materials with the vertical dimension limited in several atomic layers have aroused intense research interest in the next-generation electronic and optoelectronic applications.[1–4] Quantum confinement effects accompanied with the thickness shrinking lead to various unique material features including novel intrinsic physics and versatile application functionalities.[5,6] A series of functional 2D materials have been used as the transparent electrodes,[7] dielectric layers,[8] light absorbing layers,[9] and phototransistor channel materials,[10] playing a key role in the photodetecting areas with different device architectures.

Furthermore, the vertical heterostructures based on the layer-by-layer transfer of 2D materials are attractive for realizing efficient charge transfer interfaces with the vertical electrical fields building up, which significantly improves the photo-induced electron–hole pair separation and collection processes, in this way, the overall device quantum efficiency was increased.[11,12] However, the transfer procedures for the vertical 2D heterostructures are complicated and the use of organic adhesive polymers to assist the 2D materials stacking are inevitable, which causes the device performance to be deteriorated by residual contamination. To avoid these problems, 2D in-plane junctions (IPJs) have been developed, exhibiting promising prospects for fundamental researches and device explorations.

IPJs are generally formed by direct lateral overgrowth along the edges of the existed 2D films.[13] The advantages of the IPJ structures, such as atomically sharp in-plane interface, sub-nanometer scale band alignment engineering,[14] have been increasingly received attentions and further promoted the innovations of the IPJ fabrication technique. Specifically, the in-plane 1T/2H phase modulating under the gate voltage in the thin MoS_2 films created efficient Schottky junctions,[15] the selective chemical doping of MoS_2 flakes fulfilled in-plane p–n junctions for the diodes fabrication,[16] what is more, alternate electric doping of WSe_2 layers promotes the lateral homojunction formation to construct sensitive photodetectors.[17] These efforts have enriched the development of various IPJ structures, displaying great potentials for the future device applications.

In this work, the Bi_2O_2Se homogeneous IPJs consisting of two or more junctions with different layer thicknesses are reported, which then are adopted in the high-performance photodetectors with the metal/semiconductor/metal architecture. The Bi_2O_2Se thin film is synthesized on fluorophlogo-

*Project supported by the National Natural Science Foundation of China (Grant No. 61705066), the Open Fund of State Key Laboratory of Information Photonics and Optical Communications (Beijing University of Posts and Telecommunications), China (Grant No. IPOC2018B004), and the National Key Research and Development Program, China (Grant No. 2016YFA0202401).

†Corresponding author. E-mail: xl.liu@ncepu.edu.cn

© 2019 Chinese Physical Society and IOP Publishing Ltd

pite mica ("*f*-mica" for abbreviation) substrate for the first time by Peng *et al.* through the chemical vapor deposition (CVD) method,[18] exhibiting outstanding electrical and optoelectrical properties such as high carrier mobility,[19] narrow bandgap,[20] and ultrafast photo-response speed.[21] However, the device performance of the photodetectors based on the Bi_2O_2Se thin films is not fully explored. Especially, the device response speed is on the millisecond order[22] or several hundred microseconds,[23] which is much slower than the intrinsic picosecond scaled opto-electric process at the Bi_2O_2Se/metal interface.[21] The realization of Bi_2O_2Se homogeneous IPJs effectively builds up an internal lateral electric field at the IPJ interface due to the fact that the energy band structure of Bi_2O_2Se film is thickness-dependent,[19] which improves the photo-induced electron–hole pair dissociation efficiency. As a result, the response time of the photodetectors based on the Bi_2O_2Se IPJs is accelerated to 4.8 μs. Besides, the device photoresponsivity reaches 2.5 A/W and the detectivity 3.2×10^8 Jones (1 Jones = 1 cm·$Hz^{1/2}$·W^{-1}). Here in this work, the layer thickness modulation in the Bi_2O_2Se IPJs is realized across the *f*-mica steps which are created manually in the process of repeated peeling off the mica surface layers. Additionally, the Bi_2O_2Se films with different thicknesses can merge together, thereby the Bi_2O_2Se homojunctions are also obtained.

2. Experiment

2.1. Growth of Bi_2O_2Se in-plane homojunctions with different layer thickness

Part of the surface layers on the fluorophlogopite mica substrates, $KMg_3(AlSi_3O_{10})F_2$, were peeled away with a Scotch tape repeatedly. In this way, terraces were formed on the mica surface with a step height of about several nanometers. The Bi_2O_2Se IPJs with different layer thicknesses laterally were then obtained across the mica steps by the CVD epitaxial growth. The pre-treated mica substrates were placed at 10-cm downstream from the heating center where the Bi_2O_3 powder (purchased from Alfa Aesar, with a purity of 99.99%) was placed. The Bi_2Se_3 (with 99.999% purity supplied from Alfa Aesar) flakes were located at 7-cm upstream of Bi_2O_3. Nitrogen was used as the carrier gas and the flux was set to be 150 sccm. The pressure in the furnace was kept at 2500 Pa. The temperature of the furnace center was set to increase from room temperature (RT, 23 °C) to 580 °C in 30 min and kept at 580 °C for 60 min, then cooled down to RT naturally. The thickness and morphology of the as-grown Bi_2O_2Se IPJs were characterized with the Park XE7 AFM system.

2.2. Device fabrication and performance characterizations

The Pd/Au film with the thickness of 10 nm and 100 nm were evaporated sequentially on SiO_2/Si substrates, which was patterned with the copper TEM grids acting as the shadow masks. The Pd/Au electrodes were then fulfilled on the thinner and thicker Bi_2O_2Se IPJs layers in a peeling up and placing down procedure assisted with a probe tip under the optical microscope. The fabricated Pd/Bi_2O_2Se/Pd structures were annealed in a CVD quartz tube under a pressure of 8 Pa at 200 °C with no carrier gas.

The device performance characterizations (the electrical and optoelectronic measurements) were carried out under the vacuum condition of 10^{-3} Torr (1 Torr = 1.33322×10^2 Pa) in a Lakeshore TTPX probe station at 27 °C (300 K). The device electrical curves were obtained with the Keysight B1500 SMUs. The photo-response experiments were performed under 640-nm laser illuminating with a 1-cm^2 laser spot in diameter. The response speed of the Bi_2O_2Se IPJs was measured using a data acquisition card (NI PCIe-6321).

3. Results and discussion

The pre-treating of the mica substrates is schematically illustrated as shown in Fig. 1(a). The Scotch tape is used as the adhesive polymer to peel off the mica surface layers. Specifically, the Scotch tape sticks to the mica surface and is pressed firmly on one side of the mica, then the mica surface layers are peeled off slowly along with the scotch tape. In this way, terraces are created on the mica substrate. The Bi_2O_2Se IPJs then are synthesized through a low pressure chemical vapour deposition technique (LPCVD) similar to that in the previous reports,[18,19] which is depicted in Fig. 1(b). Across the mica terraces, a Bi_2O_2Se film is constructed by two parts with different thickness as shown in Fig. 1(c). The corresponding optical microscopic (OM) images are demonstrated in Fig. 1(g) and Fig. 2, from which the optical contrast for these two layers across the mica step is distinguishable. Besides, the Bi_2O_2Se layer on the lower mica terrace is thicker than on the higher mica terrace, which will be characterized in the following AFM results. The boundaries of mica terraces are difficult to observe under OM images because mica is highly transparent. However, the absorbance of Bi_2O_2Se in the visible spectrum is much stronger and it can be easily distinguished for the Bi_2O_2Se layers with different thicknesses.

What needs mentioning is that the Bi_2O_2Se IPJs can be formed by more than two junctions as indicated in Fig. 1(h) in a laminating growth mode. What is more, an alternative way to form Bi_2O_2Se IPJs is discovered with the neighboring (about 10 μm–20 μm distance) Bi_2O_2Se films merging together; the differences in size and orientation among these films lead to various growth speeds and the Bi_2O_2Se IPJs also consisting of layers with different thickness. The detailed IPJ formation process under this mode is illustrated in Figs. 1(d)–1(f), and the OM image of the growth results is shown in Fig. 1(i).

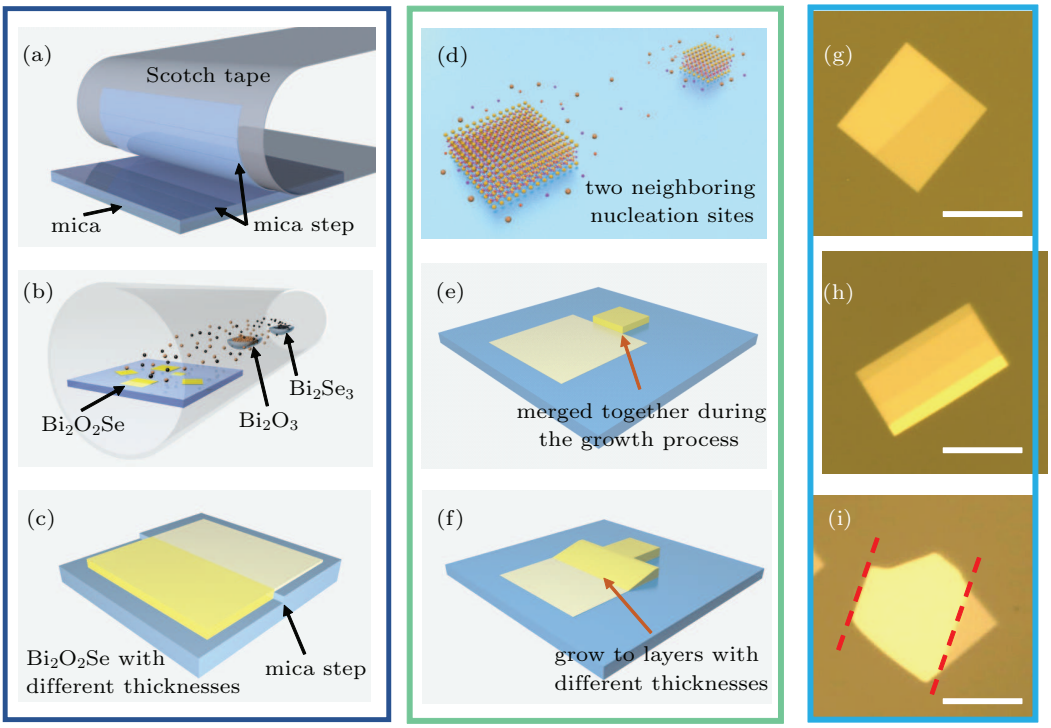


Fig. 1. (a)–(c) Schematic illustration of Bi_2O_2Se homogeneous in-plane junction fabrication process with the mica substrate pre-treating, (d)–(f) Bi_2O_2Se in-plane junction formed by near-distance nucleation sites merging together, (g) optical microscopic image of Bi_2O_2Se IPJ constructed by two layers with different thicknesses, (h) Bi_2O_2Se IPJ consisting four layers, (i) Bi_2O_2Se IPJ formed by neighboring film merging together, where red dash lines represent the parallel crystal edges of thick Bi_2O_2Se film. All scale bars are 20 μm.

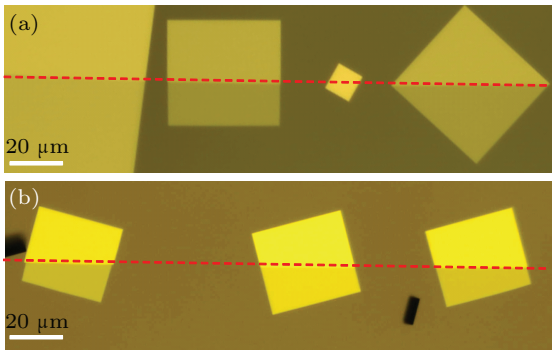


Fig. 2. The optical microscopic images of as-synthesized Bi_2O_2Se IPJs across mica steps showing ((a), (b)) three Bi_2O_2Se films affected by the same mica layer edge obviously.

With the fabricated Bi_2O_2Se IPJs, atomic force microscopy (AFM) analysis is performed to characterize the thickness information and the film morphologies. Figure 3(a) shows the OM image of a Bi_2O_2Se IPJ from which it is obviously seen that the Bi_2O_2Se square film is separated into two parts with different thicknesses along the film diagonal line. Figure 3(b) displays a corresponding AFM image of the region enclosed by the yellow square box in Fig. 3(a). From Fig. 3(b), it is clearly observed that the surface of the Bi_2O_2Se IPJ is flat. Meanwhile, there exists a mica step across the Bi_2O_2Se diagonal dividing line along the light-yellow dash line in Fig. 3(b), which, though, is difficult to observe from the OM image in Fig. 3(a), and the height information of the mica step is indicated in the lower part of Fig. 3(d). For a better demonstration, the AFM results are reconstructed with a 3D view in Fig. 3(c), in which the Bi_2O_2Se film is yellow-colored, while mica terraces separated by the step are highlighted by dark green and dark blue color. Figure 3(d) includes the height information along the yellow dash lines in Fig. 3(b), with which we could tell that the height of the thin and thick Bi_2O_2Se layers that construct the IPJ are 5 nm and 7.1 nm individually along the dark yellow dash line, besides, the mica step is 2.1-nm high along the light-yellow dash line. It is reasonable to assume that the Bi_2O_2Se nucleation and laminating growth are both energetically favorable at the adjacent mica steps, then IPJ growth can be initiated at the lower mica terrace. The surface of the Bi_2O_2Se IPJ is flat, owing to the fact that extremely low mica step ($\sim$ 2 nm) can hardly affect the Bi_2O_2Se IPJ lateral growth across the mica step, though a higher mica step (7 nm, as shown in the blue square encircled part of Fig. 4(a)) leads to a small step (0.7 nm) in the Bi_2O_2Se IPJ along the white dash line in Fig. 4(e). The AFM results in Fig. 3 reflect a fact that the Bi_2O_2Se IPJs possess good crystal quality without lattice mismatch or dislocation defects that may block the carrier transport at the IPJ interface.

What is more, another case for the Bi_2O_2Se IPJs formation is that the nearby Bi_2O_2Se films are merged together. There exists obvious difference in optical contrast in the OM image of Fig. 3(e), which represents the apparent thickness difference in the Bi_2O_2Se IPJ. The thickness information is also included in the AFM results (see Figs. 3(f) and 3(g)).

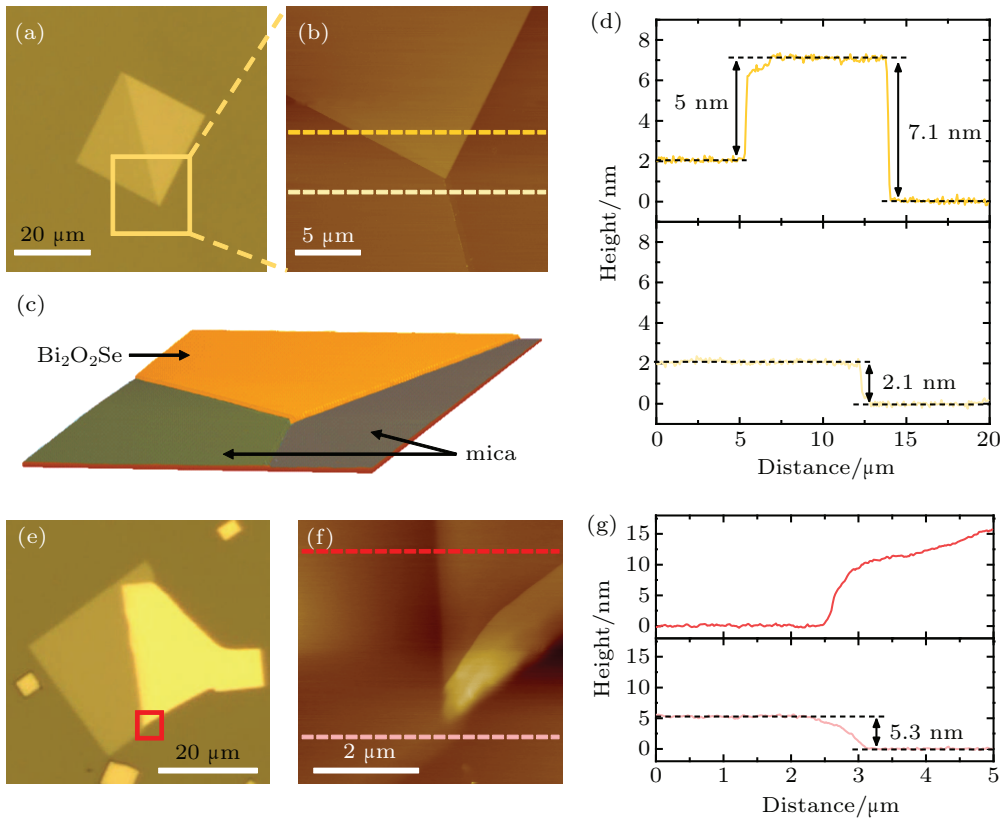


Fig. 3. (a) The OM image of a Bi_2O_2Se IPJ; (b) the AFM image of the region outlined by yellow square in panel (a); (c) the reconstructed AFM 3D image of panel (b); (d) the height profile along two yellow dash lines in panel (b); (e) the OM image of Bi_2O_2Se IPJ formed by two layers merging; (f) the AFM image of the region enclosed by red square in panel (e); (g) the height profile along red dash lines in panel (f).

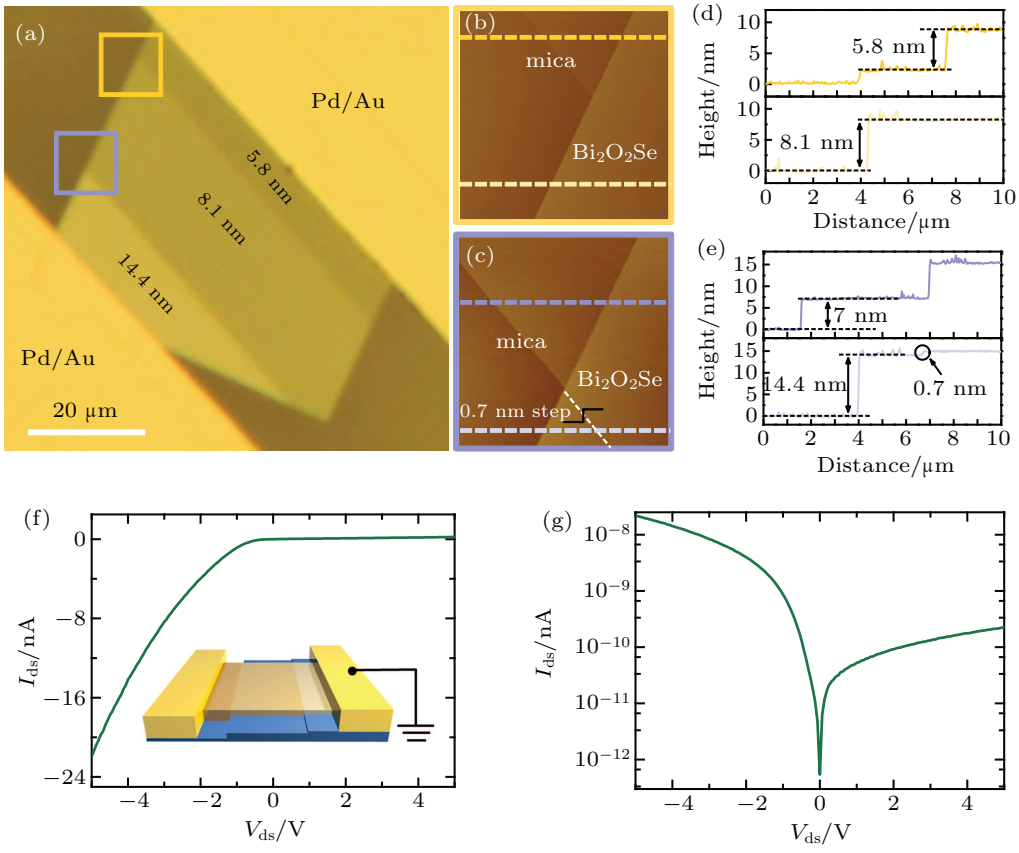


Fig. 4. (a) The OM image of as-fabricated device with 3-layered Bi_2O_2Se IPJ; (b) and (c) the AFM images of region outlined by yellow square and purple square in panel (a) respectively; (d) and (e) Height profiles along the two dash lines in panels (b) and (c); (f) and (g) the output characteristic curve of device in panel (a) with both linear and logarithmic coordinates. Inset of panel (f) shows schematic device structure.

From the AFM results, the surface of the Bi_2O_2Se IPJ under the laminating growth is continuous without dislocations, then it is believed that the corresponding optoelectronic performance is desirable owing to the fact that the effective in-plane electrical field is built up at the IPJ interface. Based on the Bi_2O_2Se IPJs with three junctions of different thicknesses, efficient photodetectors are fabricated with Pd/Au (10 nm/100 nm) serving as the electrodes. The device OM image is shown in Fig. 4(a). The devices are annealed at 200 °C in a vacuum condition to improve the metal/semiconductor contact quality and remove absorbed oxygen and water. It follows from the AFM results in Figs. 4(b) and 4(c) that the mica steps are distinguishable, and the thickness of the Bi_2O_2Se layers in the IPJs can be measured along the yellow dash lines and purple dash lines in Figs. 4(d) and 4(e), which are 14.4 nm, 8.1 nm, and 5.8 nm respectively. Correspondingly, the mica step between the thinnest Bi_2O_2Se layer and the middle layer is 2.3 nm, while the mica step between the thickest layer and the middle layer is 7 nm. A monolayer Bi_2O_2Se step of 0.7 nm is found from the lower part of Fig. 4(e), owing to the fact that the lattice parameter of Bi_2O_2Se along the [001] direction is 0.61 nm.[20] In Ref. [18], the Bi_2O_2Se monolayer (ML) is measured to be 0.8 nm. The monolayer thickness difference from the TEM[20] and the AFM results probably comes from the influences of substrates and the surface adsorbates. The device structure is depicted in the inset of Fig. 4(f), and the electrode on the thin Bi_2O_2Se layer of the IPJ is grounded for all the device measurements unless otherwise stated. The output characteristics of the device in linear and logarithmic coordinates are shown in Figs. 4(f) and 4(g), from which the diode-like current rectification behavior with a reverse/forward current ratio of 10^2 is demonstrated.

The photoresponse performance of the photodetector based on Bi_2O_2Se IPJ is characterized as shown in Fig. 5. The output curves of the device in dark and under 640-nm laser illuminating conditions are shown in Fig. 5(a). As the laser power intensity P increases from 1 mW/cm^2 to 5 mW/cm^2, the photocurrent (I_{ph}) is improved accordingly. At a forward bias voltage of -1 V, the on/off ratio between the I_{ph} at 5 mW, and the dark current is 30. Besides, at a reverse bias voltage of 1 V, the on/off ratio is about 2×10^3 that is obtained from the comparison between the I_{ph} of 96 nA and the dark current of 46 pA. The larger on/off ratio at the reverse state of the diode is attributed to the extended internal electric field at the Bi_2O_2Se in-plane junctions. The relation between the I_{ph} and P is shown in Fig. 5(b) and it could be well fitted with $I_{ph} = AP^{\alpha}$, where A and α are fitting parameters: A is 0.026 and α is 0.99. The near unity α implies the almost linear dependence of I_{ph} on incident laser power, reflecting that trap centers or defects are well controlled in the Bi_2O_2Se IPJs.[24] From Fig. 5(b), the photoresponsivity R defined as I_{ph}/P is 2.5 A/W at 5 mW/cm^2, while the detectivity D^* is 3.2×10^8 Jones from $D^* = RS^{1/2}(2eI_{dark})^{1/2}$, where S is the device area, e is the element charge, and I_{dark} is the dark current at 1 V bias voltage.

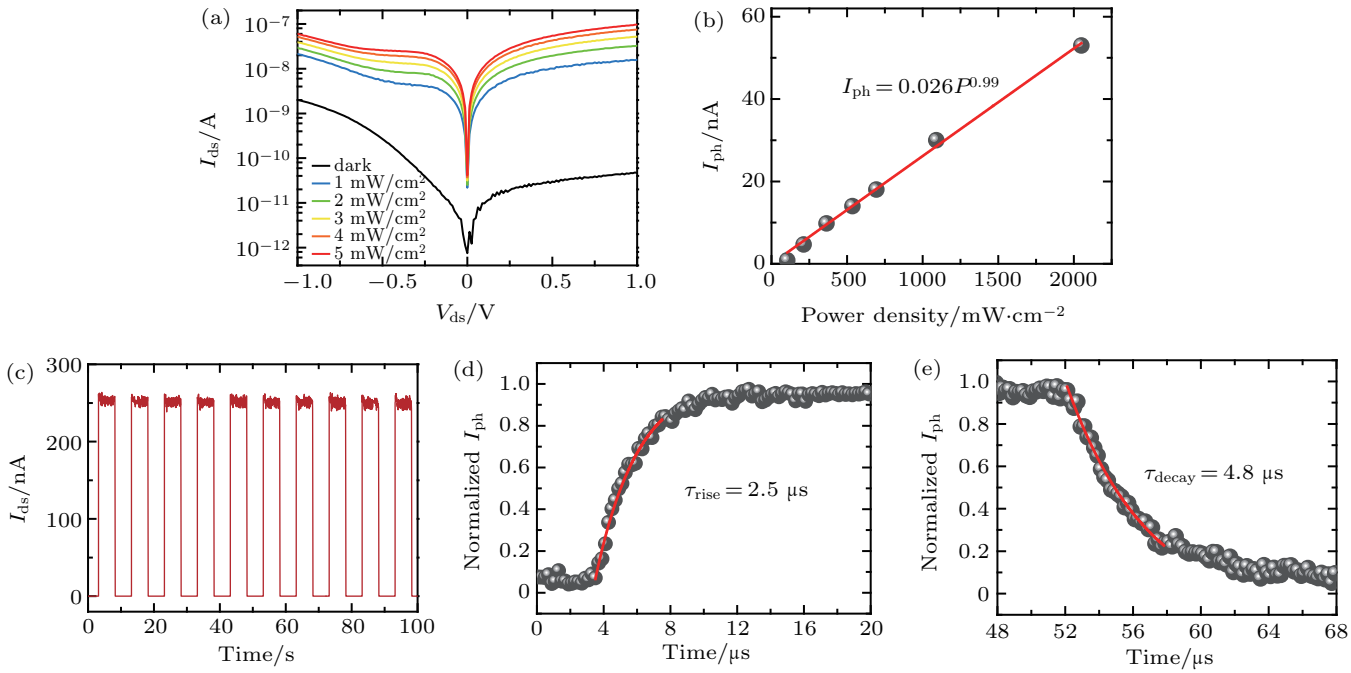


Fig. 5. (a) Output characteristics of Bi_2O_2Se IPJ in Fig. 4, demonstrating the electrical states under dark condition and 640-nm laser illumination from 1 mW/cm^2 to 5 mW/cm^2, and output curves are in logarithmic coordinates, (b) photocurrent *versus* light power density with voltage bias of 1 V, (c) time-dependent device current with 640-nm laser on/off incident modulation and voltage of 1 V, (d) and (e) single exponential fitting of dynamic response of photocurrent for (d) rise and (e) decay edges, with τ_{rise} and τ_{decay} being 2.5 μs and 4.8 μs, respectively.

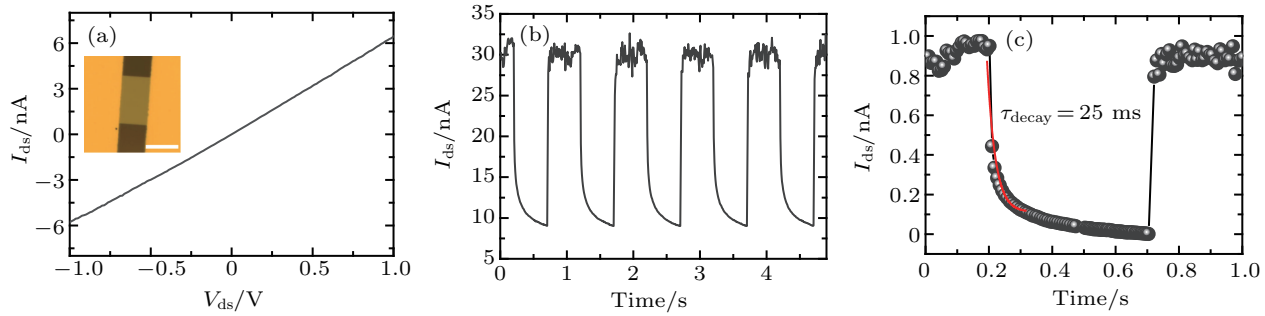


Fig. 6. (a) Output characteristic of the device based on Bi_2O_2Se uniform thin film, exhibiting Ohmic contact with the Pd/Au electrodes. Inset shows device OM image with scale bar of 20 μm, (b) time-sampling results of the device under laser on/off conditions, and (c) single exponential fitting of the decay edge with lifetime of 25 ms.

With the charge transfer states effectively formed at the IPJ interfaces between the Bi_2O_2Se layers with different thickness, the device response speed can be significantly accelerated, owing to the fact that the carrier transport routes are improved from the aspects of the light induced electron–hole pair separation, carrier drifting along the electrical fields within the IPJ, and the carrier collection by the electrodes. The Bi_2O_2Se IPJ photoresponse speed is measured under the 640-nm laser on-off modulation as indicated in Fig. 5(c). From an enlarged single I_{ph} "pulse", the rising and decay edges are fitted with single exponential functions,[25] and the lifetime is extracted to be τ_{rise} of 2.5 μs and τ_{decay} of 4.8 μs as shown respectively in Figs. 5(d) and 5(e), these values are increased by more than two orders compared with the previously published results of the photodetectors based on the Bi_2O_2Se thin films.[22,23] Yin *et al.* measured the photocarrier relaxation time at the metal-Bi_2O_2Se interface with the pump-probe technic.[21] However, there exists a large gap between the intrinsic response time at the metal-Bi_2O_2Se junction and the actual response speed of a device, which is prone to being influenced by impurities formed within the film and at the substrate/film interface acting as deep-level charge traps that will apparently reduce the device response speed by indirect electron-hole pair recombination process.

To further verify the improvement in photodetecting performance of the Bi_2O_2Se IPJ structures, reference devices based on the Bi_2O_2Se thin films with uniform layer thickness were fabricated also with Pd/Au as the electrodes. The device electrical performance is shown in Fig. 6(a) and the device OM image is displayed in the inset. The output curve of the reference device is linear and has no rectification feature, which indicates the Ohmic-type metal/semiconductor contacts and no in-plane carrier transport barriers (or specifically, there exists no internal electric field) inside the uniform Bi_2O_2Se layer. The device photoresponse is unsatisfied with R being 0.93 A/W in Fig. 6(b) and the response time is 25 ms from Fig. 6(c), which is much slower than the response time of the Bi_2O_2Se IPJ based photodetectors. The response time of MoS_2 p–n junction was 100 ms–200 ms,[26] MoS_2 and black phosphorus heterojunction was 70 μs,[27] graphene in-plane homojunction was dominated by photo-thermoelectric effect, and the device response time was not considered.[5] Compared these research results, the device response speed is greatly accelerated in Bi_2O_2Se homojunctions. Although the photoresponsivity is small in the absence of electrical gating effect in our work, it is believed that top-gated devices will exhibit higher photoresponsivity.

4. Conclusions

The Bi_2O_2Se in-plane junctions are successfully synthesized across the mica steps created by peeling off the mica surface layer. The Bi_2O_2Se IPJs are constructed by layers with different thickness, and the surface of which is flat and continuous, showing high crystal quality and laminating growth mode. Photodetectors fabricated based on the Bi_2O_2Se IPJs exhibit diode-like current rectification behavior and excellent photoresponse performance. Comparing with the devices based on the uniform Bi_2O_2Se thin films, the opto-electric conversion efficiency is improved, and the response speed is accelerated, which are attributed to the effective internal electrical field built up at the Bi_2O_2Se in-plane junction interface. We believe that the thickness modulating on the mica substrate can be applied to more 2D materials for realizing high-performance optoelectronic devices.

References

[1] Novoselov K S, Geim A K, Morozov S V, Jiang D, Zhang Y, Dubonos S V, Grigorieva I V and Firsov A A 2004 *Science* **306** 666
[2] Splendiani A, Sun L, Zhang Y, Li T, Kim J, Chim C Y, Galli G and Wang F 2010 *Nano. Lett.* **10** 1271
[3] Dean C R, Young A F, Meric I, Lee C, Wang L, Sorgenfrei S, Watanabe K, Taniguchi T, Kim P, Shepard K L and Hone J 2010 *Nat. Nanotech.* **5** 722
[4] Li L, Yu Y, Ye G J, Ge Q, Ou X, Wu H, Feng D, Chen X H and Zhang Y 2014 *Nat. Nanotech.* **9** 372
[5] Xu X, Gabor N M, Alden J S, van der Zande A M and McEuen P L 2010 *Nano Lett.* **10** 562
[6] Mak K F, Lee C, Hone J, Shan J and Heinz T F 2010 *Phys. Rev. Lett.* **150** 136805

[7] Fu X W, Liao Z M, Zhou Y B, Wu H C, Bie Y Q, Xu J and Yu D P 2012 *Appl. Phys. Lett.* **100** 223114
[8] Li H, Li X M, Park J H, Tao L, Kim K K, Lee Y H and Xu J B 2019 *Nano Energy* **57** 214
[9] Kufer D and Konstantatos G 2015 *Nano Lett.* **15** 7307
[10] Zhang W, Huang J K, Chen C H, Chang Y H, Cheng Y J and Li L J 2013 *Adv. Mater.* **25** 3456
[11] Lee C H, Lee G H, van der Zande A M, Chen W, Li Y, Han M, Cui X, Arefe G, Nuckolls C, Heinz T F, Guo J, Hone J and Kim P 2014 *Nat. Nanotech.* **9** 676
[12] Withers F, Pozo-Zamudio O D, Mishchenko A, Rooney A P, Gholinia A, Watanabe K, Taniguchi T, Haigh S J Geim A K, Tartakovskii A I and Novoselov K S 2015 *Nat. Mater.* **14** 301
[13] Qi Y, Han N, Li Y, Zhang Z, Zhou X, Deng B, Li Q, Liu M, Zhao J, Liu Z and Zhang Y 2017 *ACS Nano* **11** 1807
[14] Zheng B, Ma C, Li D, Lan J, Zhang Z, Sun X, Zheng W, Yang T, Zhu C, Ouyang G, Xu G, Zhu X, Wang X and Pan A 2018 *J. Am. Chem. Soc.* **140** 11193
[15] Katagiri Y, Nakamura T, Ishii A, Ohata C, Hasegawa M, Katsumoto S, Cusati T, Fortunelli A, Iannaccone G, Fiori G, Roche S and Haruyama J 2016 *Nano Lett.* **16** 3788
[16] Sun Q Q , Li Y J , He J L , Yang W, Zhou P, Lu H L , Ding S J and Zhang W D 2013 *Appl. Phys. Lett.* **102** 093104
[17] Groenendijk D J, Buscema M, Steele G A, Michaelis de Vasconcellos S, Bratschitsch R, van der Zant H S and Castellanos-Gomez A 2014 *Nano Lett.* **14** 5846
[18] Wu J, Yuan H, Meng M, Chen C, Sun Y, Chen Z, Dang W, Tan C, Liu Y, Yin J, Zhou Y, Huang S, Xu H Q, Cui Y, Hwang H Y, Liu Z, Chen Y, Yan B and Peng H 2017 *Nat. Nanotechnol.* **12** 530
[19] Wu J, Tan C, Tan Z, Liu Y, Yin J, Dang W, Wang M and Peng H 2017 *Nano Lett.* **17** 3021
[20] Chen C, Wang M, Wu J, Fu H, Yang H, Tian Z, Tu T, Peng H, Sun Y, Xu X, Jiang J, Schroter N B M, Li Y, Pei D, Liu S, Ekahana S A, Yuan H, Xue J, Li G, Jia J, Liu Z, Yan B, Peng H and Chen Y 2018 *Sci. Adv.* **4** eaat8355
[21] Yin J, Tan Z, Hong H, Wu J, Yuan H, Liu Y, Chen C, Tan C, Yao F, Li T, Chen Y, Liu Z, Liu K and Peng H 2018 *Nat. Commun.* **9** 3311
[22] Li J, Wang Z, Wen Y, Chu J, Yin L, Cheng R, Lei L, He P, Jiang C, Feng L and He J 2018 *Adv. Funct. Mater.* **28** 1706437
[23] Fu Q, Zhu C, Zhao X, Wang X, Chaturvedi A, Zhu C, Wang X, Zeng Q, Zhou J, Liu F, Tay B K, Zhang H, Pennycook S J and Liu Z 2019 *Adv. Mater.* **31** 1804945
[24] Fang H and Hu W 2017 *Adv. Sci.* **4** 1700323
[25] Liu X, Luo X, Nan H, Guo H, Wang P, Zhang L, Zhou M, Yang Z, Shi Y, Hu W, Ni Z, Qiu T, Yu Z, Xu J B and Wang X 2016 *Adv. Mat.* **28** 5200
[26] Choi M S, Qu D, Lee D, Liu X, Watanabe K, Taniguchi T and Yoo W J 2014 *ACS Nano* **8** 9332
[27] Ye L, Li Hao, Chen Z and Xu J B 2016 *ACS Photon.* **3** 692